

# Nonlinear magnetotransport in MoTe<sub>2</sub>

A.C. Marx,<sup>\*</sup> H. Jafari, E.K. Tekelenburg, M.A. Loi, J. Sławińska, and M.H.D. Guimarães<sup>†</sup>  
*Zernike Institute for Advanced Materials, University of Groningen, NL-9747AG Groningen, The Netherlands*

The shape of the Fermi surface influences many physical phenomena in materials and a growing interest in how the spin-dependent properties are related to the fermiology of crystals has surged. Recently, a novel current-dependent nonlinear magnetoresistance effect, known as bilinear magnetoelectric resistance (BMR), has been shown to be not only sensitive to the spin-texture in spin-polarized non-magnetic materials, but also dependent on the convexity of the Fermi surface in topological semimetals. In this paper, we show that the temperature dependence of the BMR signal strongly depends on the crystal axis of the semimetallic MoTe<sub>2</sub>. For the *a*-axis, the amplitude of the signal remains fairly constant, while for the *b*-axis it reverses sign at about 100 K. We calculate the BMR efficiencies at 10 K to be  $\chi_J^A = (173 \pm 3) \text{ nm}^2 \text{ T}^{-1} \text{ A}^{-1}$  and  $\chi_J^B = (-364 \pm 13) \text{ nm}^2 \text{ T}^{-1} \text{ A}^{-1}$  for the *a*- and *b*-axis, respectively, and we find that they are comparable to the efficiencies measured for WTe<sub>2</sub>. We use density functional theory calculations to compute the Fermi surfaces of both phases at different energy levels and we observe a change in convexity of the outer-most electron pocket as a function of the Fermi energy. Our results suggest that the BMR signal is mostly dominated by the change in the Fermi surface convexity.

The bilinear magnetoelectric resistance (BMR) effect is a powerful technique to extract important information on the band structure of quantum materials, such as Fermi surface convexity and spin textures [1–5]. The BMR effect causes a modulation of the material's resistance depending on the relative angle between applied electric and magnetic fields [6]. As the name suggests, it has a linear dependence with both current and magnetic field and, unlike the unidirectional magnetoresistance [7], it does not depend on a conducting ferromagnetic layer. This effect has been used to explore the spin-dependent Fermi surface of systems with different electronic properties [1–3], and to give information on the shape and topology of the electron and hole pockets of semimetallic systems [4].

Weyl semimetals present an interesting platform to explore new physical phenomena due to their topologically protected states [8]. These states, called Fermi arcs, appear at the surface of materials and connect the conduction and valence band [9]. A lot of work has been done in understanding the influence of the topologically protected states on the transport properties of Weyl semimetals [10–16], but a complete understanding of the role of bulk bands is still lacking.

The Weyl semimetal candidate MoTe<sub>2</sub> is a van der Waals material showing low crystal symmetry [17–19] and strong spin-orbit coupling (SOC) [20, 21]. Moreover, it undergoes a crystallographic phase transition as a function of temperature [22]. MoTe<sub>2</sub> crystallizes in the

monoclinic  $1T'$  phase at room temperature and transitions to the orthorhombic  $T_d$  phase below 240 K [22, 23] (Fig. 1a). The crystallographic lattice shows a metallic zigzag chain along the *b*-axis, leading to a strong resistance anisotropy in the *ab*-plane for both phases [23]. The phase transition also leads to a change on the crystal symmetry group, from space group  $P2_1/m$  to space group  $Pmn2_1$ , allowing for additional spintronic phenomena to occur [19, 24, 25]. It is important to note that  $1T'$ -MoTe<sub>2</sub> possesses inversion symmetry, which implies absence of band splitting and thus, a zero net (bulk) spin-texture. This results in a Fermi surface that is fully spin-degenerate. However, a non-zero spin-texture can appear at the surfaces, allowing for a "hidden" spin texture in the  $1T'$  phase [26–28]. Interestingly, the  $T_d$  phase is predicted to be a type-II Weyl state with two Weyl nodes close to the Fermi level, while the  $1T'$  phase remains a trivial semimetal [29–31]. Although a large magnetoresistance has been measured in  $T_d$ -MoTe<sub>2</sub> [10, 32, 33], the origins of the effect are not yet clear, since theoretical calculations indicate that MoTe<sub>2</sub> is an uncompensated semimetal [34]. Moreover, despite these interesting properties and promising spintronic [19, 35–37] and topological applications [11–14, 38, 39], no study of its nonlinear magnetoresistance, i.e. the BMR effect, has been performed so far.

In this work, we report on the BMR effect observed for the two main crystal axis of semimetallic MoTe<sub>2</sub> as a function of temperature. We observe a change in the BMR signal as we cool down from room temperature to 10 K which is strongly anisotropic with respect to the crystal axes (Fig. 1). For some of our devices we observe a crystal-phase change as a function of temperature, which apparently is partially correlated to the change

<sup>\*</sup> a.c.marx.goncalves@rug.nl

<sup>†</sup> m.h.guimaraes@rug.nl

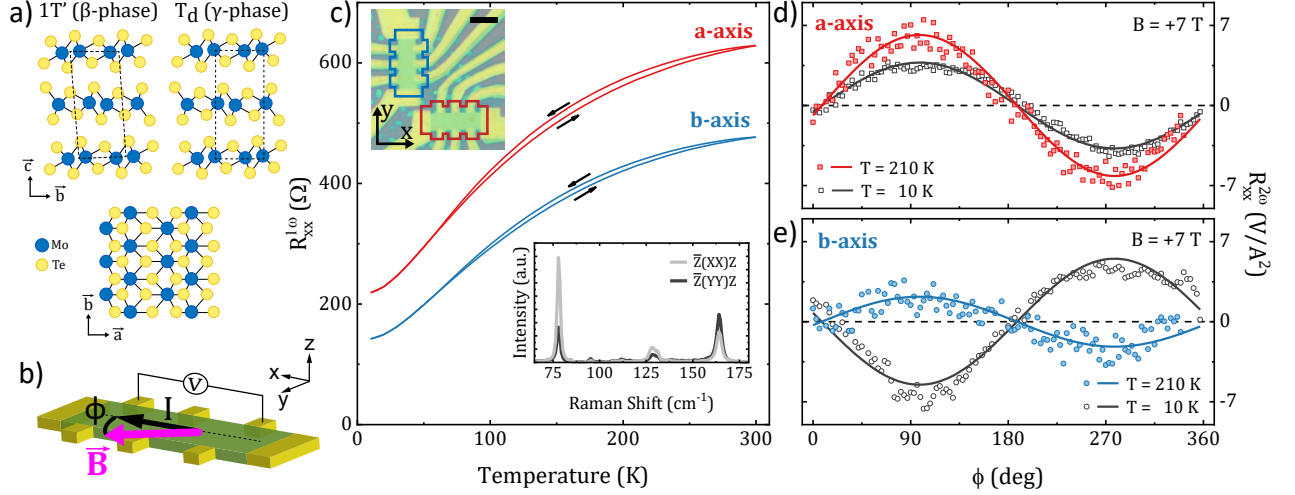


FIG. 1. (a) Crystal structure of semimetallic MoTe<sub>2</sub> in the 1T' and T<sub>d</sub> crystal phases. (b) Schematics for the bilinear magnetoelectric resistance measurements. (c) Longitudinal resistance as a function of temperature measured with the current along the two main crystal axis of MoTe<sub>2</sub>. The top inset shows an optical image of the device (scale bar corresponds to 5 μm) and the bottom inset shows the polarized Raman spectra for each axis. BMR measurements with the current applied along the a- (d) and b-axis (e) with an in-plane magnetic field of 7 T for two different temperatures (10 K and 210 K). A vertical offset was removed for clarity.

in the BMR signal. Despite this crystal phase change, density-functional theory (DFT) calculations show little changes on the overall band structure or band convexity at the Fermi level for both phases. This indicates that the strong dependence of the BMR signal we observe could be attributed to a change on the Fermi surface convexity resulting from a Fermi level shift as a function of temperature, as observed in the sister material T<sub>d</sub>-WTe<sub>2</sub> [4].

Our devices consist of 1T'-MoTe<sub>2</sub> encapsulated in hexagonal boron nitride (hBN), fabricated by mechanically exfoliated crystals (HQ Graphene), and stacked on top of each other via a dry van der Waals assembly technique [40]. The hBN/1T'-MoTe<sub>2</sub>/hBN stack is assembled and placed on a SiO<sub>2</sub>/Si substrate under a nitrogen environment to protect the MoTe<sub>2</sub> crystals from degrading. Two perpendicular Hall bars were patterned on the stack, on the same MoTe<sub>2</sub> flake, using electron-beam lithography and followed by Ti/Au contact deposition by conventional techniques. The channel of each Hall bar was designed to be aligned with one of the main axis of the crystal. The measurements were performed using conventional harmonic low-frequency (177 Hz) lock-in techniques with current biases below  $I_0 = 500$  μA in a variable-temperature insert in Helium gas. The in-plane angle ( $\phi$ ) between an external magnetic field (up to  $B = 7$  T) and the current direction was varied while measuring the second-harmonic voltage in the longitudinal direction (Fig. 1b). The measurements for the transverse direction can be found in the supplementary information. We

have measured three different sets of devices with different MoTe<sub>2</sub> thicknesses ( $t$ ). The change in the BMR signal as a function of temperature is clearly observed in two of our samples,  $t = 6$  nm and 12 nm. Here we report our findings on the sample with  $t = 12$  nm as obtained by atomic force microscopy. More details on the device fabrication and the results for other samples can be found in the supplementary information.

The complete device is shown in the top inset of Fig. 1c, outlining each Hall bar with different colors to indicate the alignment of the channel with the  $a$ - (red) and  $b$ -axis (blue). To confirm this alignment we performed polarized Raman spectroscopy measurements (bottom inset of Fig. 1c) and further characterized our sample by measuring the longitudinal (first-harmonic) resistance as function of temperature, as shown in Figure 1c. As expected, a clear resistance anisotropy is observed between the two axis, where the low-resistive  $b$ -axis is along the metallic chain. Moreover, a small hysteresis loop appears in the interval between 80–300 K as the sample is cooled down and warmed up again. This behavior has been observed in thin MoTe<sub>2</sub> flakes and confirmed to be due to a phase transition from the 1T' to the T<sub>d</sub> phase. Different than for bulk MoTe<sub>2</sub> this phase transition is not abrupt, resulting from a coexistence of the two phases, with the main crystal phase changing between the 1T' and the T<sub>d</sub> phases with temperature [41, 42].

The BMR effect arises from the interplay between the

applied current and magnetic field. Mathematically, we can express the resistance of a material by a resistance term  $R_0$ , plus a term linear on the current and magnetic field:  $IR_1(\mathbf{B})$ . For an ac-current  $I = I_0 \sin(\omega t)$  applied through the material, therefore, the longitudinal voltage can be easily written by Ohm's law, yielding:

$$V = R_0 I_0 \sin(\omega t) + \frac{1}{2} R_1 I_0^2 + \frac{1}{2} R_1 I_0^2 \sin\left(2\omega t - \frac{\pi}{2}\right) \quad (1)$$

with the first-harmonic, DC and second-harmonic components of the longitudinal voltage signal being the first, second and third terms on the right, respectively. As can be seen, both DC and  $V_{xx}^{2\omega}$  are proportional to the BMR coefficient  $R_1$ . Here we focus on the second-harmonic response, which is less prone to additional artifacts.

We observe a remarkably different behavior on the second-harmonic longitudinal resistance ( $R_{xx}^{2\omega}$ ) as a function of temperature for the two crystal axes. Here we define  $R_{xx}^{2\omega} = \frac{V_{xx}^{2\omega}}{(I_0)^2}$ . Figure 1d and e show the results for  $I_0$  parallel to the  $a$ - and  $b$ -axis, respectively, for a magnetic field of +7 T and two different temperatures (10 K and 210 K). Experimental data is represented by the scattered points, while the full lines are the corresponding fits according to:

$$R_{xx}^{2\omega} = \Delta R_{xx}^{2\omega} \sin[2(\phi + \phi_0)] + y_0, \quad (2)$$

where  $\Delta R_{xx}^{2\omega}$  is the amplitude of the signal, and  $\phi_0$  and  $y_0$  are the angular and vertical offsets, respectively. For both axes we notice that  $R_{xx}^{2\omega}$  shows a sinusoidal behaviour with a periodicity of  $2\pi$ . Regions of high and low resistance states can be found at angles of about  $90^\circ$  and  $180^\circ$ . This agrees with a picture of a BMR signal arising from a Rashba-like spin-texture for the Fermi surface of  $\text{MoTe}_2$ . Strikingly, the two axes show very different behaviours as the temperature is reduced. For the  $a$ -axis, we observe only a small difference between the amplitudes at 10 K and 210 K, while for the  $b$ -axis the amplitude is not only  $\sim 2.5$  times larger at 10 K, but it also changes sign compared to the measurement at 210 K.

In order to elucidate the origins of the different behavior for the two crystal axes, we perform similar measurements at various temperatures, inset of Fig. 2. Interestingly,  $\Delta R_{xx}^{2\omega}$  remains fairly constant for the  $a$ -axis, while for the  $b$ -axis the amplitude goes from positive to negative as the temperature decreases. We note that  $\Delta R_{xx}^{2\omega}$  can strongly depend on the specific device geometry and on the temperature dependence of the resistivity. In order to exclude such effects, we calculate the BMR efficiency, defined as:

$$\chi_J = \frac{2\Delta R_{xx}^{2\omega} w t}{R_0 B}, \quad (3)$$

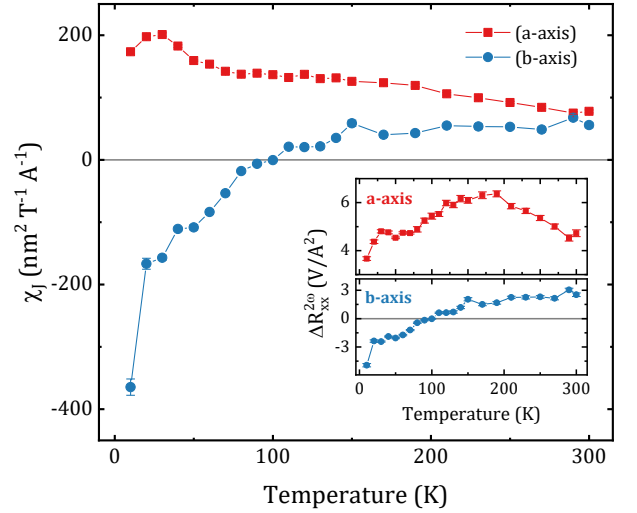


FIG. 2. The efficiency  $\chi_J$  for the current applied along the  $a$ - and  $b$ -axis as a function of temperature. The inset shows the amplitude  $\Delta R_{xx}^{2\omega}$  of the fittings for the second-harmonic resistance measurements.

with  $w$  being the channel width. The values for the BMR efficiency as a function of temperature are plotted in Figure 2. We see that  $\chi_J$  reaches similar and positive values for both the  $a$ - and  $b$ -axes at high temperatures. As the temperature decreases, the BMR efficiency increases modestly for the  $a$ -axis, peaking around 30 K. Differently,  $\chi_J$  decreases drastically for the  $b$ -axis, crossing zero at around 100 K. Cooling down further, the BMR efficiency drops rapidly for the  $b$ -axis and at 10 K we obtain a BMR magnitude of twice as large as the one for the  $a$ -axis. The computed values are  $\chi_J^A = (173 \pm 3) \text{ nm}^2 \text{ T}^{-1} \text{ A}^{-1}$  and  $\chi_J^B = (-364 \pm 13) \text{ nm}^2 \text{ T}^{-1} \text{ A}^{-1}$  for the  $a$ - and  $b$ -axes, respectively. These values and temperature behavior are comparable to the ones reported for the sister material  $\text{WTe}_2$  [4]. However, we point out that different from  $\text{MoTe}_2$ ,  $\text{WTe}_2$  does not undergo a crystal phase transition with a change in temperature. The results for  $\text{WTe}_2$  were explained as a change in the convexity of the electron pockets as a function of the Fermi level [4]. Nonetheless, it is known that BMR can also depend on the spin texture of the Fermi surfaces [1–3].

To further understand the origins of the behavior we observe, we performed DFT calculations to compute the Fermi contours of the hole and electron bands at different Fermi levels and for both crystal phases. Details of the calculations can be found in the supplementary material. As shown in Fig. 3a, the overall electronic dispersion presents some similar features for both  $1T'$  and  $T_d$  phases. Both show a semimetallic behavior, with electron and hole pockets at the Fermi level. Due to the presence

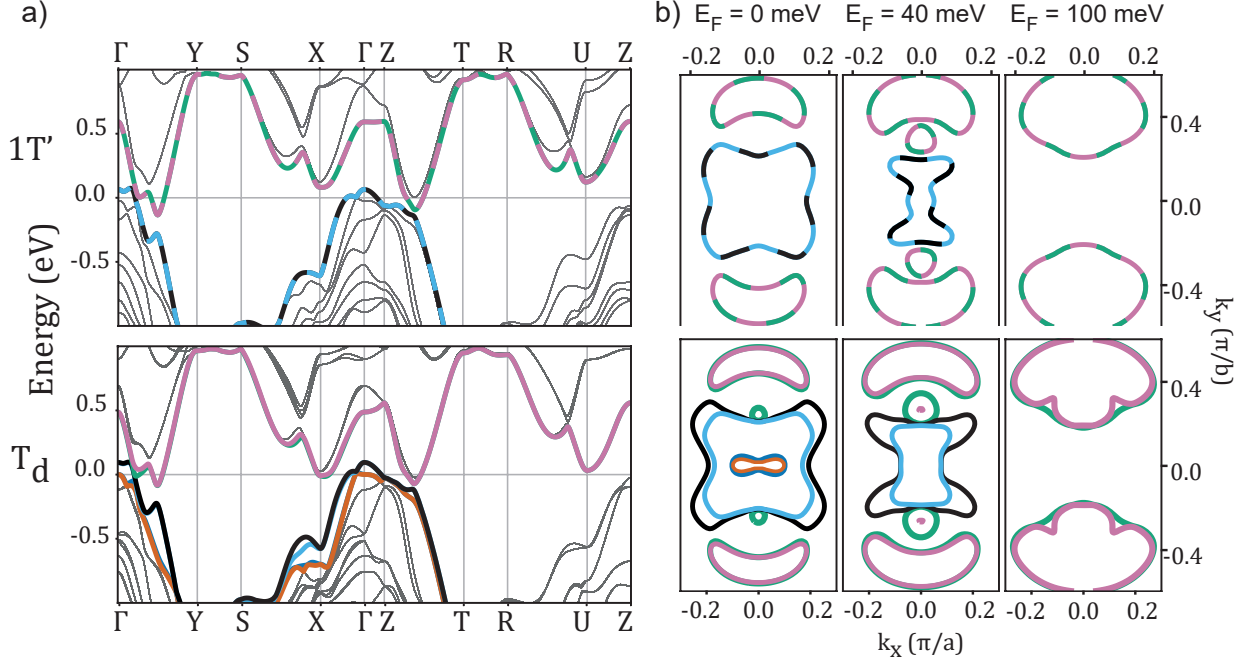


FIG. 3. **(a)** Electronic dispersion for the  $1T'$  and  $T_d$  phases, and **(b)** corresponding Fermi surfaces at different energy cuts in respect to the conduction bands:  $E_F = 0$  meV, 40 meV and 100 meV. For the bands (and corresponding Fermi surfaces) of the  $1T'$  phase, the mixing of two colours represents the spin degenerate bands.

of inversion symmetry in the  $1T'$  phase, we do not see any spin splitting in the DFT calculations. However, the  $T_d$  lacks inversion symmetry and shows a Rashba-like spin texture, i.e. with the spins perpendicular to the crystal momentum (see supplementary material for the spin-dependent electronic dispersion). For this reason, we rule out that the BMR signal is dominated by a spin-dependent contribution, since the second-harmonic signal reverses sign with temperature which would imply a reversal on the spin direction.

Similar to  $WTe_2$ , it has been demonstrated that  $MoTe_2$  can show a shift on the Fermi level as a function of temperature [43–46]. To explore the implications of this to our measurements, we obtain the Fermi-surfaces at different energies (Fig. 3) for both phases. The overall behaviour of the electron and hole pockets with the change in energy is similar for both  $1T'$  and  $T_d$   $MoTe_2$ , however the latter shows two extra hole pockets appearing at low energies. Remarkably, we obtain a change in convexity of the electron pockets for both phases along the  $\Gamma - Y$  direction. This change in convexity is consistent with the sign change we observe in our measurements, revealing that our measurements are dominated by a change in the Fermi surface convexity.

Our observations of a BMR signal dominated by the Fermi-surface convexity in  $MoTe_2$  are an important step

for the understanding of the band structure of this Weyl semimetal candidate. Here we report an anisotropic behavior of the BMR signal as a function of temperature, with a clear inversion below 100 K for the current along the  $b$ -axis while no sign reversal is observed for the current along the  $a$ -axis. This observation is in agreement with a change in the Fermi surface convexity, induced by a change in the Fermi level due to temperature, similar to what has been reported for the sister material  $WTe_2$  [4]. The fact that  $MoTe_2$  undergoes a crystal phase transition between an inversion asymmetric to an inversion symmetric one, allows us to rule out contributions from the spin texture in our BMR signals. We envision that our demonstration of large BMR signals in  $MoTe_2$  can be exploited in spintronic devices consisting of  $MoTe_2$  interfaced with two-dimensional magnets, for which the magnetic field role could be played by the magnetic exchange. This would allow one to obtain important information on the magnetization direction even on magnetic insulators, while also exploiting the unusual spin torque symmetries [19] provided by  $MoTe_2$  for magnetization manipulation.

## ACKNOWLEDGEMENTS

We thank J.G. Holstein, H. Adema, H. de Vries, A. Joshua and F.H. van der Velde for their technical support. This work was supported by the Dutch Re-

search Council (NWO) through grants STU.019.014, the Zernike Institute for Advanced Materials, the research program “Materials for the Quantum Age” (QuMat, registration number 024.005.006), which is part of the Gravitation program financed by the Dutch Ministry of Education, Culture and Science (OCW), and the European Union (ERC, 2DOPTOSPIN, 101076932). Views and

opinions expressed are however those of the author(s) only and do not necessarily reflect those of the European Union or the European Research Council. Neither the European Union nor the granting authority can be held responsible for them. The device fabrication and nanocharacterization were performed using Zernike NanoLabNL facilities.

- 
- [1] P. He, S. S.-L. Zhang, D. Zhu, Y. Liu, Y. Wang, J. Yu, G. Vignale, and H. Yang, Bilinear magnetoelectric resistance as a probe of three-dimensional spin texture in topological surface states, *Nature Physics* **14**, 495 (2018).
  - [2] P. He, S. M. Walker, S. S.-L. Zhang, F. Y. Bruno, M. S. Bahramy, J. M. Lee, R. Ramaswamy, K. Cai, O. Heinonen, G. Vignale, F. Baumberger, and H. Yang, Observation of out-of-plane spin texture in a SrTiO<sub>3</sub>(111) two-dimensional electron gas, *Physical Review Letters* **120**, 266802 (2018).
  - [3] Y. Zhang, V. Kalappattil, C. Liu, M. Mehraeen, S. S.-L. Zhang, J. Ding, U. Erugu, Z. Chen, J. Tian, K. Liu, J. Tang, and M. Wu, Large magnetoelectric resistance in the topological Dirac semimetal  $\alpha$ -Sn, *Science Advances* **8**, eabo0052 (2022).
  - [4] P. He, C.-H. Hsu, S. Shi, K. Cai, J. Wang, Q. Wang, G. Eda, H. Lin, V. M. Pereira, and H. Yang, Nonlinear magnetotransport shaped by Fermi surface topology and convexity, *Nature Communications* **10**, 1290 (2019).
  - [5] T. Liu, A. Roy, J. Hidding, H. Jafari, D. K. De Wal, J. Sławińska, M. H. D. Guimarães, and B. J. Van Wees, Crystallographically dependent bilinear magnetoelectric resistance in a thin WTe<sub>2</sub> layer, *Physical Review B* **108**, 165407 (2023).
  - [6] S. Zhang and G. Vignale, Theory of bilinear magnetoelectric resistance from topological-insulator surface states, in *Spintronics XI* (SPIE, San Diego, United States, 2018) p. 40.
  - [7] C. O. Avci, K. Garello, A. Ghosh, M. Gabureac, S. F. Alvarado, and P. Gambardella, Unidirectional spin Hall magnetoresistance in ferromagnet/normal metal bilayers, *Nature Physics* **11**, 570 (2015).
  - [8] A. A. Burkov, Topological semimetals, *Nature Materials* **15**, 1145 (2016).
  - [9] K. Deng, G. Wan, P. Deng, K. Zhang, S. Ding, E. Wang, M. Yan, H. Huang, H. Zhang, Z. Xu, J. Denlinger, A. Fedorov, H. Yang, W. Duan, H. Yao, Y. Wu, S. Fan, H. Zhang, X. Chen, and S. Zhou, Experimental observation of topological Fermi arcs in type-II Weyl semimetal MoTe<sub>2</sub>, *Nature Physics* **12**, 1105 (2016).
  - [10] F. C. Chen, H. Y. Lv, X. Luo, W. J. Lu, Q. L. Pei, G. T. Lin, Y. Y. Han, X. B. Zhu, W. H. Song, and Y. P. Sun, Extremely large magnetoresistance in the type-II Weyl semimetal MoTe<sub>2</sub>, *Physical Review B* **94**, 235154 (2016).
  - [11] X. Qian, J. Liu, L. Fu, and J. Li, Quantum spin Hall effect in two-dimensional transition metal dichalcogenides, *Science* **346**, 1344 (2014).
  - [12] Y. Zhang, J. Van Den Brink, C. Felser, and B. Yan, Electrically tuneable nonlinear anomalous Hall effect in two-dimensional transition-metal dichalcogenides WTe<sub>2</sub> and MoTe<sub>2</sub>, *2D Materials* **5**, 044001 (2018).
  - [13] F. C. Chen, X. Luo, J. Yan, Y. Sun, H. Y. Lv, W. J. Lu, C. Y. Xi, P. Tong, Z. G. Sheng, X. B. Zhu, W. H. Song, and Y. P. Sun, Planar Hall effect in the type-II Weyl semimetal T<sub>d</sub>-MoTe<sub>2</sub>, *Physical Review B* **98**, 041114 (2018).
  - [14] Y. Zhang, Y. Sun, and B. Yan, Berry curvature dipole in Weyl semimetal materials: An *ab initio* study, *Physical Review B* **97**, 041101 (2018).
  - [15] S. Khim, K. Koepernik, D. V. Efremov, J. Klotz, T. Förster, J. Wosnitza, M. I. Sturza, S. Wurmehl, C. Hess, J. Van Den Brink, and B. Büchner, Magnetotransport and de Haas-van Alphen measurements in the type-II Weyl semimetal TaIrTe<sub>4</sub>, *Physical Review B* **94**, 165145 (2016).
  - [16] G. Sharma, P. Goswami, and S. Tewari, Chiral anomaly and longitudinal magnetotransport in type-II Weyl semimetals, *Physical Review B* **96**, 045112 (2017).
  - [17] K. Zhang, C. Bao, Q. Gu, X. Ren, H. Zhang, K. Deng, Y. Wu, Y. Li, J. Feng, and S. Zhou, Raman signatures of inversion symmetry breaking and structural phase transition in type-II Weyl semimetal MoTe<sub>2</sub>, *Nature Communications* **7**, 13552 (2016).
  - [18] S.-Y. Chen, T. Goldstein, D. Venkataraman, A. Ramasubramaniam, and J. Yan, Activation of new Raman modes by inversion symmetrybreaking in type II Weyl semimetal candidate T'-MoTe<sub>2</sub>, *Nano Letters* **16**, 5852 (2016).
  - [19] G. M. Stiehl, R. Li, V. Gupta, I. E. Baggari, S. Jiang, H. Xie, L. F. Kourkoutis, K. F. Mak, J. Shan, R. A. Buhrman, and D. C. Ralph, Layer-dependent spin-orbit torques generated by the centrosymmetric transition metal dichalcogenide  $\beta$ -MoTe<sub>2</sub>, *Physical Review B* **100**, 184402 (2019).
  - [20] C. H. Naylor, W. M. Parkin, J. Ping, Z. Gao, Y. R. Zhou, Y. Kim, F. Streller, R. W. Carpick, A. M. Rappe, M. Drndić, J. M. Kikkawa, and A. T. C. Johnson, Monolayer single-crystal 1T'-MoTe<sub>2</sub> grown by chemical vapor deposition exhibits weak antilocalization effect, *Nano Letters* **16**, 4297 (2016).
  - [21] J. Cui, P. Li, J. Zhou, W.-Y. He, X. Huang, J. Yi, J. Fan, Z. Ji, X. Jing, F. Qu, Z. G. Cheng, C. Yang, L. Lu,

- K. Suenaga, J. Liu, K. T. Law, J. Lin, Z. Liu, and G. Liu, Transport evidence of asymmetric spin-orbit coupling in few-layer superconducting  $1T_d$ -MoTe<sub>2</sub>, *Nature Communications* **10**, 2044 (2019).
- [22] R. Clarke, E. Marseglia, and H. P. Hughes, A low-temperature structural phase transition in  $\beta$ -MoTe<sub>2</sub>, *Philosophical Magazine B* **38**, 121 (1978).
- [23] H. P. Hughes and R. H. Friend, Electrical resistivity anomaly in  $\beta$ -MoTe<sub>2</sub> (metallic behaviour), *Journal of Physics C: Solid State Physics* **11**, L103 (1978).
- [24] A. Roy, M. H. D. Guimarães, and J. Ślawińska, Unconventional spin Hall effects in nonmagnetic solids, *Physical Review Materials* **6**, 045004 (2022).
- [25] K. Tenzin, A. Roy, H. Jafari, B. Banas, F. T. Cerasoli, M. Date, A. Jayaraj, M. Buongiorno Nardelli, and J. Ślawińska, Analogs of Rashba-Edelstein effect from density functional theory, *Physical Review B* **107**, 165140 (2023).
- [26] Q. Liu, X. Zhang, and A. Zunger, Intrinsic circular polarization in centrosymmetric stacks of transition-metal dichalcogenide compounds, *Physical Review Letters* **114**, 087402 (2015).
- [27] H. Yuan, M. S. Bahramy, K. Morimoto, S. Wu, K. Nomura, B.-J. Yang, H. Shimotani, R. Suzuki, M. Toh, C. Kloc, X. Xu, R. Arita, N. Nagaosa, and Y. Iwasa, Zeeman-type spin splitting controlled by an electric field, *Nature Physics* **9**, 563 (2013).
- [28] J. M. Riley, F. Mazzola, M. Dendzik, M. Michiardi, T. Takayama, L. Bawden, C. Granerød, M. Leandersson, T. Balasubramanian, M. Hoesch, T. K. Kim, H. Takagi, W. Meevasana, Ph. Hofmann, M. S. Bahramy, J. W. Wells, and P. D. C. King, Direct observation of spin-polarized bulk bands in an inversion-symmetric semiconductor, *Nature Physics* **10**, 835 (2014).
- [29] Y. Sun, S.-C. Wu, M. N. Ali, C. Felser, and B. Yan, Prediction of Weyl semimetal in orthorhombic MoTe<sub>2</sub>, *Physical Review B* **92**, 161107 (2015).
- [30] Z. Wang, D. Gresch, A. A. Soluyanov, W. Xie, S. Kushwaha, X. Dai, M. Troyer, R. J. Cava, and B. A. Bernevig, MoTe<sub>2</sub> : A type-II Weyl topological metal, *Physical Review Letters* **117**, 056805 (2016).
- [31] J. Jiang, Z. Liu, Y. Sun, H. Yang, C. Rajamathi, Y. Qi, L. Yang, C. Chen, H. Peng, C.-C. Hwang, S. Sun, S.-K. Mo, I. Vobornik, J. Fujii, S. Parkin, C. Felser, B. Yan, and Y. Chen, Signature of type-II Weyl semimetal phase in MoTe<sub>2</sub>, *Nature Communications* **8**, 13973 (2017).
- [32] S. Lee, J. Jang, S.-I. Kim, S.-G. Jung, J. Kim, S. Cho, S. W. Kim, J. Y. Rhee, K.-S. Park, and T. Park, Origin of extremely large magnetoresistance in the candidate type-II Weyl semimetal MoTe<sub>2-x</sub>, *Scientific Reports* **8**, 13937 (2018).
- [33] Q. L. Pei, W. J. Meng, X. Luo, H. Y. Lv, F. C. Chen, W. J. Lu, Y. Y. Han, P. Tong, W. H. Song, Y. B. Hou, Q. Y. Lu, and Y. P. Sun, Origin of the turn-on phenomenon in  $T_d$ -MoTe<sub>2</sub>, *Physical Review B* **96**, 075132 (2017).
- [34] S. Thirupathaiah, R. Jha, B. Pal, J. S. Matias, P. K. Das, P. K. Sivakumar, I. Vobornik, N. C. Plumb, M. Shi, R. A. Ribeiro, and D. D. Sarma, MoTe<sub>2</sub> : An uncompensated semimetal with extremely large magnetoresistance, *Physical Review B* **95**, 241105 (2017).
- [35] S. Lim, C. R. Rajamathi, V. Süß, C. Felser, and A. Kapitulnik, Temperature-induced inversion of the spin-photogalvanic effect in WTe<sub>2</sub> and MoTe<sub>2</sub>, *Physical Review B* **98**, 121301 (2018).
- [36] C. K. Safeer, N. Ontoso, J. Ingla-Aynés, F. Herling, V. T. Pham, A. Kurzmam, K. Ensslin, A. Chuvilin, I. Robredo, M. G. Vergniory, F. De Juan, L. E. Hueso, M. R. Calvo, and F. Casanova, Large multidirectional spin-to-charge conversion in low-symmetry semimetal MoTe<sub>2</sub> at room temperature, *Nano Letters* **19**, 8758 (2019).
- [37] J. Zhou, J. Qiao, A. Bournel, and W. Zhao, Intrinsic spin Hall conductivity of the semimetals MoTe<sub>2</sub> and WTe<sub>2</sub>, *Physical Review B* **99**, 060408 (2019).
- [38] X. Luo, F. C. Chen, J. L. Zhang, Q. L. Pei, G. T. Lin, W. J. Lu, Y. Y. Han, C. Y. Xi, W. H. Song, and Y. P. Sun,  $T_d$ -MoTe<sub>2</sub>: A possible topological superconductor, *Applied Physics Letters* **109**, 102601 (2016).
- [39] S. Singh, J. Kim, K. M. Rabe, and D. Vanderbilt, Engineering Weyl phases and nonlinear Hall effects in  $T_d$ -MoTe<sub>2</sub>, *Physical Review Letters* **125**, 046402 (2020).
- [40] P. J. Zomer, M. H. D. Guimarães, J. C. Brant, N. Tombros, and B. J. Van Wees, Fast pick up technique for high quality heterostructures of bilayer graphene and hexagonal boron nitride, *Applied Physics Letters* **105**, 013101 (2014).
- [41] R. He, S. Zhong, H. H. Kim, G. Ye, Z. Ye, L. Winford, D. McHaffie, I. Rilak, F. Chen, X. Luo, Y. Sun, and A. W. Tsien, Dimensionality-driven orthorhombic MoTe<sub>2</sub> at room temperature, *Physical Review B* **97**, 041410 (2018).
- [42] Y. Cheon, S. Y. Lim, K. Kim, and H. Cheong, Structural phase transition and interlayer coupling in few-layer  $1T'$  and  $T_d$  MoTe<sub>2</sub>, *ACS Nano* **15**, 2962 (2021).
- [43] Y. Wu, N. H. Jo, M. Ochi, L. Huang, D. Mou, S. L. Bud'ko, P. C. Canfield, N. Trivedi, R. Arita, and A. Kaminski, Temperature-induced Lifshitz transition in WTe<sub>2</sub>, *Physical Review Letters* **115**, 166602 (2015).
- [44] N. Xu, Z. W. Wang, A. Magrez, P. Bugnon, H. Berger, C. E. Matt, V. N. Strocov, N. C. Plumb, M. Radovic, E. Pomjakushina, K. Conder, J. H. Dil, J. Mesot, R. Yu, H. Ding, and M. Shi, Evidence of a Coulomb-interaction-induced Lifshitz transition and robust hybrid Weyl semimetal in  $T_d$ -MoTe<sub>2</sub>, *Physical Review Letters* **121**, 136401 (2018).
- [45] S. Beaulieu, S. Dong, N. Tancogne-Dejean, M. Dendzik, T. Pincelli, J. Maklar, R. P. Xian, M. A. Sentef, M. Wolf, A. Rubio, L. Rettig, and R. Ernstorfer, Ultrafast dynamical Lifshitz transition, *Science Advances* **7**, eabd9275 (2021).
- [46] D. Kim, J.-H. Lee, K. Kang, D. Won, M. Kwon, S. Cho, Y.-W. Son, and H. Yang, Thermomechanical Manipulation of Electric Transport in MoTe<sub>2</sub>, *Advanced Electronic Materials* **7**, 2000823 (2021).